Journal of Heat and Mass Transfer Research 10 (2023) 31 - 42

Semnan University

Journal of Heat and Mass Transfer Research

Journal homepage: https://jhmtr.semnan.ac.ir

Research Article

Numerical Investigation of the Separation of Microparticles inside the Microchannel Using the Vortices Caused by the ICEK Phenomenon

Seyed Mohammad Ehsan Ghadamgahi, Mohammad Mohsen Shahmardan, Mohsen Nazari *, Hamed Mansouri

Faculty of Mechanical Engineering, Shahrood University of Technology, Shahrood, iran.

PAPER INFO

Paper history:

Received: 2023-02-17

Revised: 2023-07-07

Accepted: 2023-07-08

Keywords:

Induced charged electrokinetic;

Microfluidics;

Microparticles;

Separation;

Floating electrode.

ABSTRACT

One field of study in microfluidics is the control, trapping, and separation of microparticles suspended in fluid. In recent years, much research has been started in this field. Some of its applications are related to cell handling, viruses, and bacteria detection, checking and analyzing biological cells and DNA molecules, testing water quality, or checking impurities in water. One of the new methods in this field is using Induced-charge electrokinetic phenomena (ICEK) and dielectrophoresis force. In the Induced-charge electrokinetic phenomena, the property of polarization of a conductive surface located in an electric field causes vortices to be created on the conductive plate in the fluid. This conductive plate is called a floating electrode. In the present study, considering the Induced-charge electrokinetic phenomena, the dielectrophoresis force, and creating an outlet on the roof of the microchannel at the place where two vortices of the ICEK phenomenon meet (secondary outlet), the microparticles inside the fluid are separated in the desired ratio. The separation is such that after the microparticles reach the floating electrode, they are trapped in the ICEK flow vortex and separated through a secondary channel, which is placed crosswise and non-coplanar above the main channel. In the present study, yeast microparticles are suspended in a KCl electrolyte solution and injected into the microchannel by a syringe pump. The arbitrary adjustment of the percentage of conduction and separation of microparticles towards the secondary outlet by adjusting the parameters of the applied voltage and fluid inlet velocity to the microchip is one of the innovations of the present study. In the simulation results, we observed that for input velocities (20-120) (μm)/s, respectively, with applied voltages (150-330) V (to create an electric field in the floating electrode), 100% of the particles can be directed towards the secondary-outlet, and separated. To validate the simulation results, the results obtained from the simulation method of the present study have been compared with the results of previous works.

DOI: 10.22075/jhmtr.2023.29957.1419

1. Introduction

The Development of science in micro and nano fluids is progressing rapidly due to its basic applications. One area of study is the control, trapping, separating and directing of micro/nanoparticles suspended in fluid, which has been the subject of much research in recent years. Some of its applications are cell, virus, and bacteria handling or detection, examining and analyzing biological cells and DNA molecules, assembling nano and microparticles to make equipment in these dimensions, testing water quality [1], and so on.

*Corresponding Author: Mohsen Nazari.
Email: mnazari@shahroodut.ac.ir

In this field, several techniques/methods are applied, such as optical tweening, electrophoresis, and dielectrophoresis. Most of the studies in this field have been done with these methods. However, each of these methods has its limitations. The optical tweening method is the most common method of trapping individual particles [2], but it requires expensive and advanced laser equipment [3]. The electrophoresis method can only be used to move electrically charged particles [4].

The dielectrophoresis method can be used to separate and trap particles [5]. In this method, the electrodes are designed in such a way that they create a non-uniform electric field, and this field creates a dielectrophoresis force. This method is being developed, and new ideas are being introduced, the amount of dielectrophoresis force changes drastically with the change of electrical properties, shape, and size of particles. This issue can limit the use of dielectrophoresis force. Sometimes, the combination of the mentioned factors makes it necessary to apply high voltage and frequency to the electrodes to create enough force to affect the particles, which will destroy living cells [6, 32].

In the present work, the Induced-charge electrokinetic phenomena method on the polarizable conductive plate (floating electrode) is used to guide the particles toward the secondary channel. The Induced-charge electrokinetic phenomena method is a new tool in nano and micro fluids to trap or separate particles [7].

A conductive plate, which can be polarized, created this phenomenon [8]. In the ICEK phenomenon, the conductive plate is located in an external electric field. By creating an electric double layer by dissolved ions that are in contact with the surface of the floating electrode, the Induced-charge electrokinetic phenomena occur and create vortices on the surface of the electrode. The charge amount of the conductive surface or zeta potential can be adjusted by changing the external electric field. According to the classical Helmholtz-Smoluchowski formula, particle/fluid velocity induction is non-linearly and directly dependent on the external electric field. A typical application for this method is to mix fluids in micro-dimensions. Other applications of this method include water quality testing, micro flow control, electrolyte demixing, micro pumps, and nano and micro fluid regulation to control ion transfer, such as rectifier flow [9]. Other new applications include particle separation, transport, trapping, and concentration. It is also used to examine cells [11, 10], viruses [12], and other microscopic organisms [13]. This method can also be used to manufacture nano and micro equipment [14].

Applying this method is straightforward because the fluid flow is created using two external electrodes at both ends of the microchannel that create an electrical field. These electrodes are called driver electrodes. Created fluid flow can be used from electroosmotic flow, an external pump or a syringe.

Although certain techniques are employed to improve the mixing or trapping of particles, etc. in Microfluidic systems, they may lead to a rise in solution temperature or apply a rise in the electrical field. Consequently, such methods are unsuitable for biological purposes since certain biological samples are highly susceptible to temperature changes. method of the present study decreases these cases [14,35,37].

In 2018, Zhao and Yang were able to trap suspended particles in the electrolyte solution by combining AC and DC electric fields in a microchannel with a conducting strip that can be polarized [15]. In 2013, Shao and Liu et al. created gold nanowires inside an electrolyte solution by using the chain effect in gold nanoparticles [16]. In 2016, Ren and Wu et al. designed a microchip to trap particles or cells individually on floating electrodes using the ICEO phenomenon [17]. In 2015, Ren, Liu, and Jia et al. developed a method to control the location of particle concentration on a floating electrode. In their method, the concentration of the particles is controlled on the surface of the electrode by adjusting the amount of potential applied to the floating electrode [18]. In 2016, Ren, Liu, and Tao et al. presented a method for particle concentration, that by using the vortices created on the floating electrode in the ICEO phenomenon, the particles trapped in the direction of the fluid flow and the center line of the electrode [19]. In 2016, Ren and Liu et al. presented a method that separated a stream of particles at the desired ratio after trapping the particles in the center line of the microchannel along the fluid flow [20]. In 2016, Li and Song et al. presented a method; that particles concentrated in a limited area after passing through two ICEO vortices created on two floating electrodes facing each other [21]. In 2018, Zhao and Yang trapped nano-particles and micro-particles inside a continuous flow on the end edge of a floating electrode [22]. In 2017, Chen et al., by using floating electrodes in the direction of the microchannel and on its bottom, using ICEK vortices, concentrated the particles in the center line of the microchannel and then with the electrodes that were attached to it using dielectrophoresis force. First, microparticles deviated to the left or right wall of the microchannel then the particles were diverted to one of the desired outlets at its end [1]. In 2013, Din et al. created chains of nanoparticles by using the ICEK phenomenon and rhomboid floating electrodes and using high frequencies in driver electrodes [23]. In 2019, Chen and colleagues separated two different types of particles from the two outlets at the end of the microchannel by using the vortices created in the Induced-charge electrokinetic phenomena and asymmetric electrodes embedded in the direction of the fluid flow and on the bottom of the microchannel [24].

In 2021, Nazari and colleagues designed an electroosmotic micro pump using an electric field gradient and asymmetric microelectrodes [25]. Also, in 2020, they were able to design a microchip to produce micro drops in a microchannel using a proportional-integral-derivative controller with the ability to adjust the flow rate of micro drops [26]. In 2022, Tavari, Nazari and colleagues discussed Different electrokinetic mechanisms implemented in electrohydrodynamic-, electroosmosis-, electrothermal, electrophoresis and dielectrophoresis-based micro pumps [30]. In 2022, Tavari, Nazari and colleagues optimized the geometrical parameters of electrodes, such as the width and height of steps on each base electrode and their location in one pair, the size of each base electrode (symmetric or asymmetric), and the gap of electrode pairs [31]. In 2022, Nazari M and colleagues showed that the mixing efficiency can be enhanced significantly as a micro-mixer with conductive mixing-enclosure is employed [32]. In 2020, Nazari M and colleagues simulated an induced-charge electrokinetic micro-mixer with a flexible conductive plate, they showed that the vortices created around the flexible plate are larger than the vortices of the non-flexible plate due to plate deformation [33]. In 2011, Daghighi Y and colleagues studied the transient induced-charge electrophoretic (ICEP) motion of a Janus particle in a microchannel. In their, effects of the applied electric field, size of the particle, and zeta potential of the non-polarizable part on the motion of Janus particle are also studied [34]. In 2022, Nazari M and colleagues numerically studied an electrokinetic micro-mixer with an inductive load. They performed a comprehensive geometrical study on this micro-mixer and investigated the effects of various parameters [35]. In 2017, Azimi S and colleagues studied a micro-mixer based on the continuous deformation of a flexible conductive link. Since this link is conductive, once the electric field is applied, vortices form around the link. Applying a time-varying DC electric field causes variation in the applied forces to the link; thus, the link will swipe the channel and acts as a micro-stirrer to enhance mixing results [36]. In 2020, Nazari M and colleagues proposed a new design of an electrokinetic micro-mixer with an inductive load that had a mixing chamber with conductive surfaces. In their study, the effects of conductive edges, mixing-chamber size, and electric field strength on the mixing process and mass transfer are investigated [37].

In the present study, a microchip was designed that can the microparticles trapped and directed to a secondary outlet by the vortices of the ICEK phenomenon. Considering that the rotation of both vortices is opposite to each other and the location of the selected outlet is in the area where the two vortices collide, the microparticles are directed to that area. Adjusting the inlet velocity and the applied voltage allows a desired percentage of the particles to be directed and separated in the direction of the secondary outlet. This adjustable separation using a simple microchip design is one of the innovations of this study.

2. Theory and Mathematical Model

2.1. Electric Field and Fluid Flow Equations

The governing equation for AC electric potential can be derived from Maxwell's equations. The subscript f corresponds to the fluid, and the subscript p corresponds to the particle.

$$\nabla.\left(\tilde{\varepsilon}_f \nabla\tilde{\varphi}\right) = 0 \qquad \text{in fluid} \tag{1}$$

$$\nabla.\left(\tilde{\varepsilon}_p \nabla\tilde{\varphi}\right) = 0 \qquad \text{in the space inside the particle} \tag{2}$$

Complex electric potential ($\tilde{\varphi}$) and complex relative permittivity ($\tilde{\varepsilon}$) are shown below.

$$\tilde{\varphi} = \varphi(\vec{x})e^{j\omega t} \tag{3}$$

$$\tilde{\varepsilon}_p = \varepsilon_p - j\frac{\sigma_p}{\omega} \tag{4}$$

$$\tilde{\varepsilon}_f = \varepsilon_f - j\frac{\sigma_f}{\omega} \tag{5}$$

in the above equations, ε is the permittivity coefficient, σ is the electrical conductivity, and ω is the angular frequency, which has a linear relationship with the frequency as $\omega = 2\pi f$. At low frequencies, electrical conductivity plays a dominant role, and at high frequencies, permittivity plays a dominant role.

The electric field $\tilde{\vec{E}}$ in the system is calculated by the following equation [21, 19].

$$\tilde{\vec{E}} = -\nabla\tilde{\varphi} \tag{6}$$

In viscous and unsteady fluid flow for an incompressible and Newtonian fluid in a laminar state, Continuity and Navier-Stokes equations are used, which are expressed as follows [21, 19].

$$\rho\left[\frac{\partial\vec{u}}{\partial t} + (\vec{u}.\nabla)\vec{u}\right] = -\nabla\vec{P} + \mu\nabla\vec{u} + \vec{f}_B \qquad \text{in fluid} \tag{7}$$

$$\nabla.\vec{u} = 0 \qquad \text{in fluid} \tag{8}$$

in the mentioned equations, ρ is the fluid density,$\vec{u}$ is the fluid velocity, $\vec{P}$ is fluid pressure, μ is dynamic fluid viscosity, and $\vec{f}_B$ is volumetric fluid force.

2.2. Calculation of Dielectrophoresis Force Using Point Dipole Method

In this method, the particles are assumed to be point dipole spheres. This method calculates the dielectrophoresis force for DC electrical current in the following equation [19].

$$\vec{F}_{DEP} = 2\pi\varepsilon_f R^3 Re(f_{CM}).\nabla\left(\vec{E}.\vec{E}\right) \tag{9}$$

$$f_{CM} = \frac{\varepsilon_p - \varepsilon_f}{\varepsilon_p + 2\varepsilon_f} \quad (10)$$

in the above relations, R is the particle radius, and f_{CM} is the Clausius-Mossotti factor. If the real part of the Clausius-Mossotti factor is positive, the particle moves towards the stronger electric field. The dielectrophoresis force created is called the positive dielectrophoresis force. Nevertheless, if the real part of the Clausius-Mossotti factor is negative, the particle moves towards the weaker electric field, and a negative dielectrophoresis force is created. If the applied field is an AC field, the dielectrophoresis force is expressed as a time average [18, 19, 27].

$$\langle \vec{F}_{DEP} \rangle = 2\pi\varepsilon_f R^3 Re(f_{CM}).\nabla(\vec{E}_0.\vec{E}_0) \quad (11)$$

2.3. Equations Related to Induced-Charge Electrokinetic Phenomena

By applying a voltage to the driving electrode, ions accumulate on the border of the floating electrode with the electrolyte solution. This layer created from ions is called an induced double layer[1]. After the passage of a specific time, called the characteristic RC time scale and expressed by the relation (12), the double layer's surface capacity is charged [18].

$$\tau_{RC} = \frac{\bar{\bar{r}} C_d}{\sigma(1+\delta)} = \varepsilon\bar{\bar{r}}/\sigma\,\lambda_D(1+\delta) \quad (12)$$

$\bar{\bar{r}}$ is the size characteristic of the shape, and in this study, it is equal to 0.195L. Here, L is the dimension of the electrode along the channel. This double layer of ions has Debye length, which is expressed by the relation (13). The characteristic frequency of the time scale is also expressed by the relation (14) [19, 18].

$$\lambda_D = \sqrt{D\varepsilon/\sigma} \quad (13)$$

$$f_{RC-average} = \frac{\sigma(1+\delta)}{2\pi\bar{\bar{r}}C_d} \quad (14)$$

D is ionic diffusivity expressed in the m^2/s unit, σ is the conductivity of the electrolyte, and ε is electrolyte permittivity or the fluid's ability to store electrical energy in an electric field. This double layer makes the surface of the floating electrode act like a complete electric field insulator. The change in the angle of the electric field on the floating electrode creates two vortices by applying force on the ions; the opposition of these vortices creates a region suitable for trapping particles [23, 19].

The conductivity of electrolyte fluid was assumed to be homogeneous; the governing equation of the electric field is simplified from equation (6) to Laplace's equation.

$$\nabla^2\tilde{\varphi} = 0 \quad (15)$$

If the electric field alternates with frequency ω, $\tilde{\varphi} = Acos(\omega t + \theta)$, the range of charging capacity of the double layer is obtained by the relation (16) [23,19].

$$\sigma(n.\nabla\tilde{\varphi}) = j\omega\frac{C_d}{(1+\delta)}\left(\tilde{\varphi} - \tilde{V}_0\right) \quad (16)$$

in this equation, $\tilde{V}_0$ is the surface potential of the floating electrode and $\tilde{\varphi}$ is the potential of the electrolyte fluid at the outer boundary of the double layer. n is the unit normal vector from the electrode to the outside (fluid). Also, $C_0 = \frac{C_d}{(1+\delta)}$ the interfacial total capacitance is the ratio of the diffuse layer $C_d = \varepsilon/\lambda_D$ to the stern layer near the surface $C_S = 0.2\,F/m^2$. As a result, the surface physical capacitance is equal to $\delta = C_d/C_S$.

After obtaining the $\tilde{\varphi}$ equation, in the second step to solve the ICEO flow rate on the floating electrode, the Navier-Stokes equations related to the creeping flow and the continuity equation were put into the Helmholtz-Smoluchowski equation and the equation (17) was obtained [15, 26, 20].

$$\begin{aligned}\langle u_{slip} \rangle &= \frac{-\varepsilon}{\mu}\langle \zeta E_t \rangle = \frac{-\varepsilon}{\mu}\frac{1}{2}Re\left(\tilde{\zeta}\tilde{E}_t{}^*\right) \\ &= \frac{\varepsilon}{2\mu(1+\delta)}Re\left(\left(\tilde{\varphi} - \tilde{V}_0\right)\left(\tilde{E} - \tilde{E}.n.n\right)^*\right)\end{aligned} \quad (17)$$

Which $\tilde{\zeta} = \frac{(\tilde{V}_0 - \tilde{\varphi})}{(1+\delta)}$ is called induced zeta potential. The symbol $\langle\ \rangle$ is the time average value for the alternating field. The sign $Re(\dots)$ means the real part of the parameter inside the parenthesis. The star is also a complex conjugate operator [18, 23, 19].

The non-slip boundary condition is established on both surfaces of the electrodes on the sides of the floating electrode (with potential V and ground) and other insulation boundaries. Boundary conditions related to electrical equations are as follows.

$$\tilde{\varphi} = \varphi(\vec{x}) \qquad \text{at the electrode surface} \quad (18)$$

$$\vec{n}.(\nabla\tilde{\varphi}) = 0 \qquad \text{In insulating surfaces} \quad (19)$$

in the above equation, $\vec{n}$ is a vector perpendicular to the surface.

The continuity of electric potential and vertical flux of electric field density at the common boundary of particle and fluid is expressed as follows [19].

[1] IDL

$$\tilde{\varphi}_p = \tilde{\varphi}_f \quad (20)$$

$$\varepsilon_p \frac{\partial \tilde{\varphi}_p}{\partial \vec{n}} = \varepsilon_f \frac{\partial \tilde{\varphi}_f}{\partial \vec{n}} \quad (21)$$

2.4. Movement of Particles

The transfer speed of particles is expressed according to Newton's second law.

$$m_p \frac{d\vec{u}_p}{dt} = \vec{F}_{net} \quad (22)$$

m_p is the particle's mass, and $\vec{F}_{netp}$ is the force applied to the particle, expressed by the equation (23).

$$\vec{F}_{netp} = \int \acute{\sigma}_p \cdot \vec{n} d\Gamma \quad (23)$$

Γ is the particle's surface, and $\acute{\sigma}_p$ is the stress tensor applied to it, expressed according to equation (24).

$$\acute{\sigma}_p = -p\acute{I} + \mu[\nabla\vec{u} + (\nabla\vec{u})^T] \quad (24)$$

in the above equation, $\acute{I}$ is the unit stress tensor of the second order [21].

For spherical particles, the rotation term does not affect the concentration and direction of the particles, and these three equations (23) to (25) are used to describe the movement of particles. Nevertheless, if the particles are non-spherical, the rotation equations should also be used.

Equation (26) expresses the rotational speed of the particles.

$$I_p \frac{d\vec{\omega}_p}{\partial t} = \vec{T}_{net} \quad (25)$$

I_p is the moment of inertia of the particle, and $\vec{T}_{netp}$ is the total torque applied to the particle and is defined by the following equation [16].

$$\vec{T}_{netp} = \int (\vec{x}_S - \vec{x}_p) \times (\acute{\sigma}_p \cdot \vec{n}) d\Gamma \quad (26)$$

The following equations determine the location of the particle.

$$\vec{x}_p = \vec{x}_{p0} + \int_0^t \vec{u}_p dt \quad (27)$$

$$\theta_p = \vec{\theta}_{p0} + \int_0^t \vec{\omega}_p dt \quad (28)$$

$\vec{x}_{p0}$, and $\vec{\theta}_{p0}$ are the initial location and angle of the initial placement of the particle, respectively [21].

3. Materials and Methods

3.1. Chip Design

A microchip is designed to guide microparticles inside the electrolyte fluid using the induced-charge electrokinetic phenomena and accounting for the dielectrophoresis force, as shown in Figure 1.

A microchannel with dimensions of 1000 × 100 µm is created. Then, three electrodes are placed microchannel. The first electrode, at the inlet microchannel, has a potential of V. The middle electrode, with a width of 250 µm, which is polarized by the applied electric field, is called a floating electrode and causes the vortices of the induced electrokinetic phenomenon. This electrode is placed in the middle of the distance between the two surrounding electrodes.

Moreover, the end electrode is located at the main outlet and has ground potential. From above the floating electrode, a secondary outlet with a width of 10 µm is designed (Figure 1). This outlet is responsible for separating and directing particles from the flow inside the main channel. The electrodes around the floating electrode with V and zero voltage that provide the electric field necessary for the floating electrode to be polarized are called driver electrodes.

The dimensions of the electrodes are shown in Figure 1. When the floating electrode is polarized, a double layer of ions is created on its surface, and ICEK vortices are formed. Electrolyte fluid containing microparticles is injected into the microchip with a syringe pump.

Figures 1 show the inlet and outlets from the beginning and end of the main channel and an output from above of floating electrode.

The electrolyte fluid used is KCL aqueous solution with electrical conductivity $\sigma = 0.001S$, with relative permittivity equal to 80, and yeast cell particles with a diameter of 1 micrometers are used as microparticles.

In driver electrodes, V volts are applied to the primary electrode, and the end electrode is considered the ground. The generated electric field polarizes the floating electrode. The fluid flow enters the microchannel with a velocity of $\vec{u}$. In the present study, the effect of changes in input velocity ($\vec{u}$) and voltage (V) on the percentage of particles directed to the secondary oulet has been investigated.

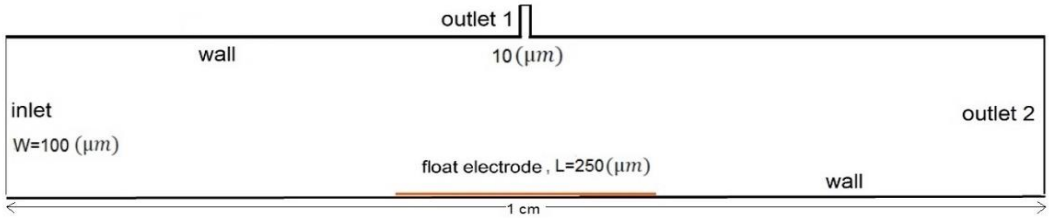

Figure 1. Microchannel design: Dimensions of the channel, the floating electrode and the outlet 1 location for particle trapping., placement of electrodes, and location of input and outlets

4. Results and Discussion

4.1. Numerical Solution Results

The microchannel design for simulation is shown in Figure 1. The characteristics of particles and fluid are specified in the previous section (Steps and how to perform the test). When the particles reach the vortices on the floating electrode, if the strength (size) of the vortices is greater than the inertia of the movement of the particles, they are directed to the secondary outlet. However, If the kinetic inertia or speed of the particles is greater than the power of the vortices to trap them, the particles will pass through the main outlet (Figure 2). As shown in Figure 3, a certain percentage of particles are directed into the secondary channel for each input voltage and inlet velocity. According to the contour shown, the desired percentage of particle separation can be reached by adjusting the input voltage and inlet velocity. Also, increasing the value of the input voltage (or decreasing the inlet velocity) leads to the dominance of the vortices. It increases the probability of trapping particles in the secondary outlet (Figures 4 and 5). The simulation is done by existing software. The equations used in three sections are 1- fluid flow equations, 2- electrical equations and 3- particle tracing to solve the movement path of microparticles inside the fluid. Fluid flow and electric field equations are done according to the equations mentioned in section 2.1, and dielectrophoresis force equations are done according to the equations of section 2.2. The electrical boundary condition on the floating electrode is based on equation 16 and the boundary condition related to the fluid flow section in the floating electrode is based on equation 17. The fluid flow is obtained by applying the boundary conditions and governing equations and is calculated using the equations of section 2.4 of the movement of microparticles in the fluid. Also, Figure 9 shows the governing equations and boundary conditions on the microchip schematicConclusion may review the main points of the author work. Also, it could include application of proposed method and suggestion for feature research.

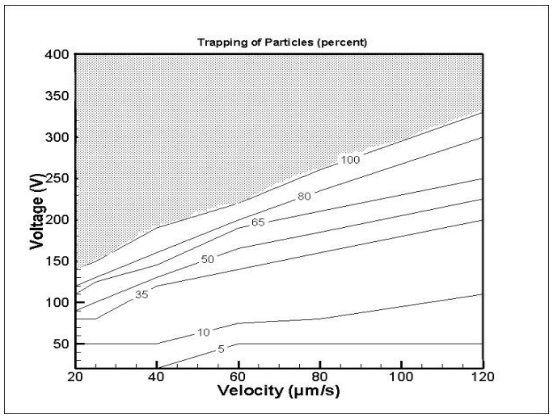

Figure 3. Particle trapping percentage for the range of voltage $V = 20 - 330\ V$ and inlet velocity $\vec{u} = 20 - 120\ \frac{\mu m}{s}$

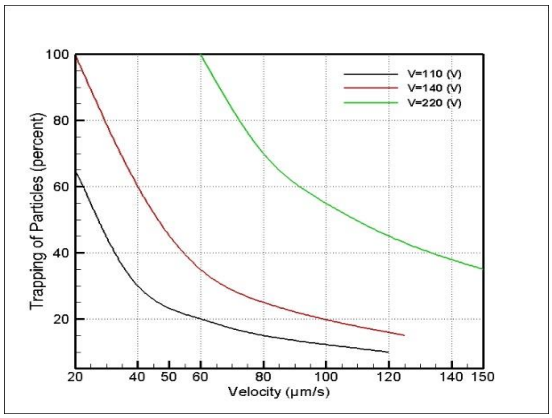

Figure 4. Particle trapping percentage by changing the inlet velocity at applied voltages of 110, 140, and 220 volts

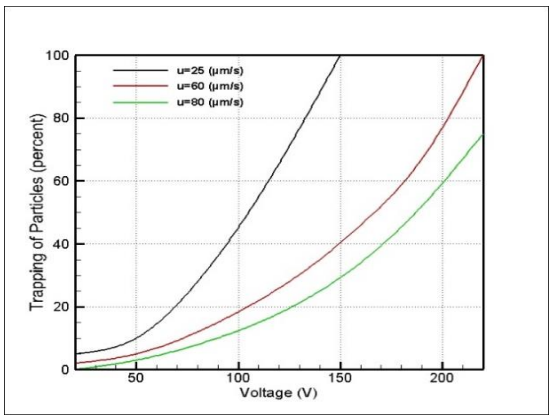

Figure 5. Particle trapping percentage by changing the applied voltages at inlet velocities of 25, 60, and 80 $\frac{\mu m}{s}$

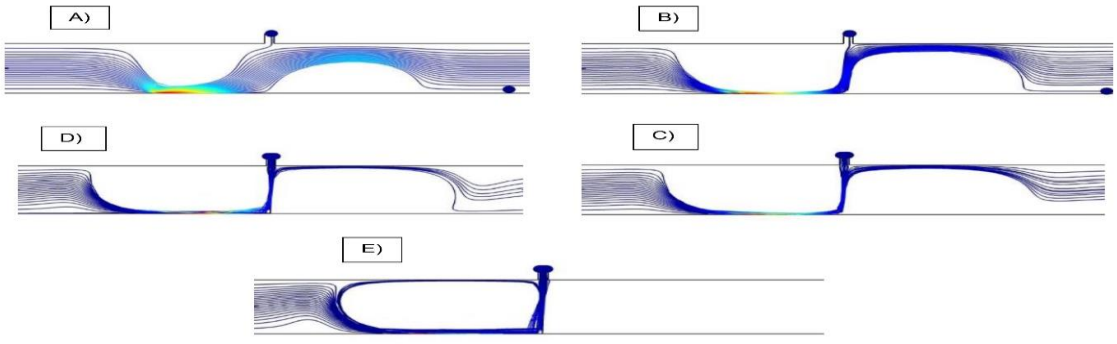

Figure 2. Creation of ICEK vortices on the floating electrode and particle trajectories when $\vec{u} = 25\ \frac{\mu m}{s}$ A) $V = 20\ V$, B) $V = 50\ V$, C) $V = 80\ V$ D) $V = 110\ V$, and E) $V = 150\ V$

4.2. Validation of Numerical Solution

To ensure the correctness of the numerical solution method of this study, first, some of the experiments or simulations done in the previous articles are re-simulated, and the results are compared. Figure 6A shows the microchip design depicted in Song et al.'s [21] article. Their test fluid is pure water with electrical conductivity $6_m = 5.5\,\mu S/m$. The width, height, and length of the microchannel are 50 μm, 1100 μm, and 1 cm, respectively, and are made of PDMS, and the length of the floating electrode is 250 μm, made of copper. The applied electric field is $E = 200\,V/cm$. The value of the induced zeta potential on the surface of the floating electrode in work done in the aforementioned article has been compared with its values from the simulation results of the numerical method of this study. Figure 6B shows a good agreement (less than 2%) between the present simulation results and the article results.

Figure 7A shows the microchip design in the study done by Ren et al. [18]. The length of the microchannel is 3 mm, and the length of the floating electrode is 200 μm. The electrodes are made of Indium Tin Oxide and are placed in a glass substrate. The thickness of the electrodes is 220 nm with a resistance of 6.5-6.8 ohms. Its ability to store electrical energy (permittivity) is equal to $\varepsilon = 7.08 \times 10^{-10}\,F/m$. The aqueous solution of KCL electrolyte has electrical conductivity $6_m = 0.0008\,S/m$. In Figure 7B, the value of the velocity of the fluid on the electrode surface (as a result of the ICEK phenomenon), extracted from the results in the article mentioned above, is compared with the numerical solution of the present study. Here, too, there is a good agreement (with an error of less than 2%) between the results.

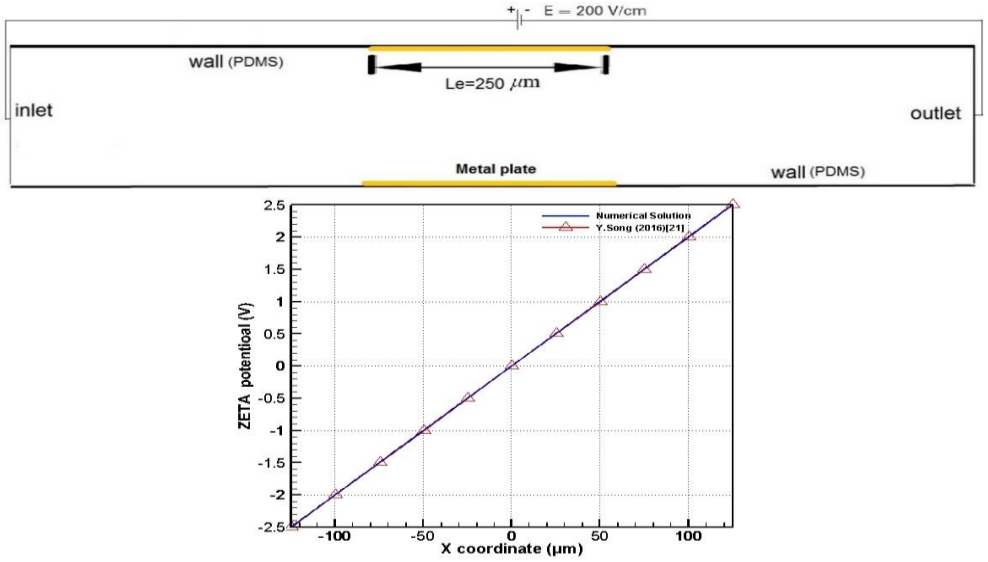

Figure 6. A) The microchip design in the article by Song et al.[21], B) Comparison of the induced zeta potential value on the electrode surface in the article by Song et al.[21] and the present simulation ($E_0 = 200\,V/cm$)

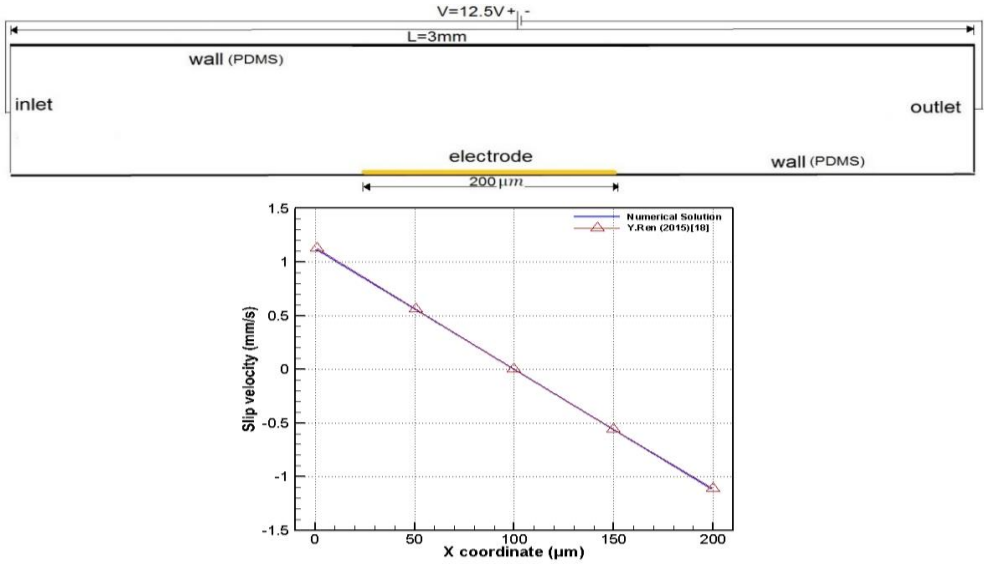

Figure 7. A) The microchip design of Ren et al.'s article [18], B) Comparison of the slip velocity value on the electrode surface in Ren et al.'s article [18] with the simulation of the present study

Figure 8A shows the microchannel design of Wu Z et al.'s article [28, 29]. In Figures 8B and 8C, the values of speed and zeta potential induced on the floating electrode obtained from the numerical simulation method of the current study are compared with the results of the mentioned article. The length of the microchannel is 20 mm, its width is 300 μm, and the floating electrode is a triangular surface with a base of 250 μm and a height of 125 μm. The fluid used is an aqueous solution of KCL electrolyte. The applied electric field is $E_0 = 25\,V/cm$. As can be seen in this figure, there is a good agreement (less than 10%) between the results in the two cases mentioned.

According to the mentioned validations, the numerical method used in the present study obtained correct results which was used to carry out the numerical simulation of the present study.

4.2.1. *Investigating Grid Independence, Particle Movement in Vortices, Equations, and Boundary Conditions of Numerical Solution*

To check the independence of the numerical solution grid used in the present study, a comparison of the movement path of a microparticle in the microchannel when the number of grids is changed has been used. The optimal grid to use in the numerical solution is the smallest number of grids in case the results do not change with increasing the number of grids.

Figure 10 shows the movement path of particles in the microchannel with a different number of grids. These results were obtained for the design shown in Figure 1 at a voltage of 80 V and an input speed of 25 $\frac{\mu m}{s}$.

In this case, KCL electrolyte fluid, polystyrene microparticles, and their diameter of 1 μm are considered. The dimensions of the channel and the floating electrode are shown in Figure 1, and the boundary conditions and equations of the problem are shown in Figure 9. Outlet 1 is for trapping particles.

As shown in Figure 10, the results for grid number 9011 have changed compared to the results for grid number 38621, but the results for grid number 38621 are in perfect agreement with the results for grid number 92950. Therefore, with the increase in the number of the grid, no change has been made in the results.

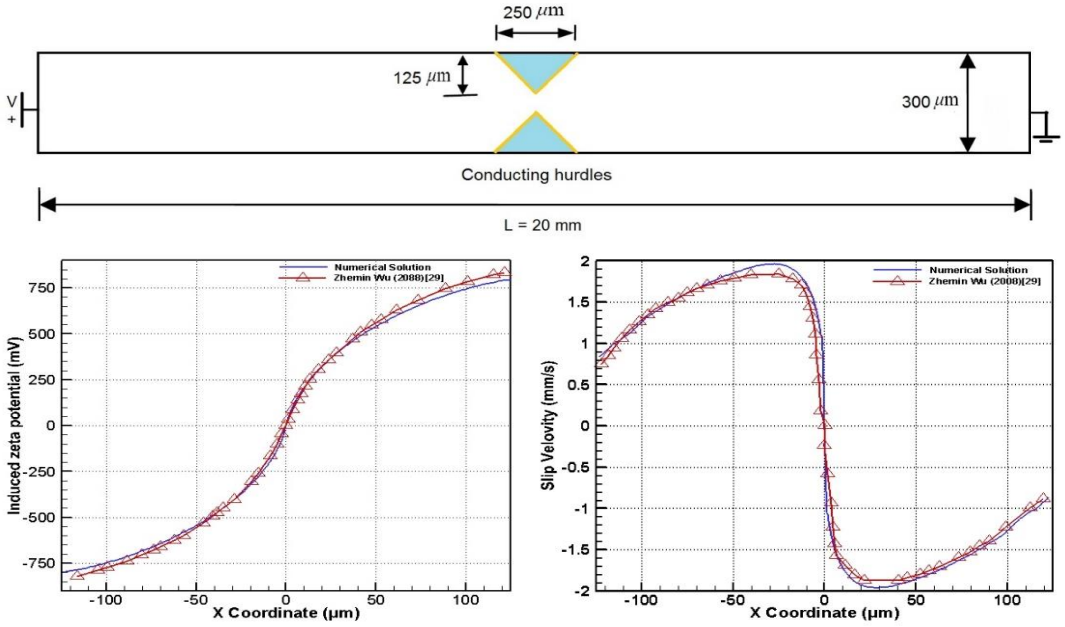

Figure 8. A) microchip design of the study done in reference [28], B) comparison of induced zeta potential values, C) comparison of the slip velocity on the floating electrode of the current numerical solution with reference [28] ($E_0 = 25\,V/cm$)

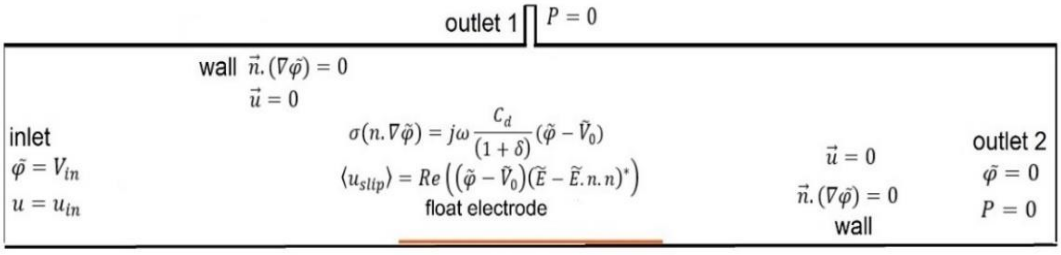

Figure 9. Boundary conditions

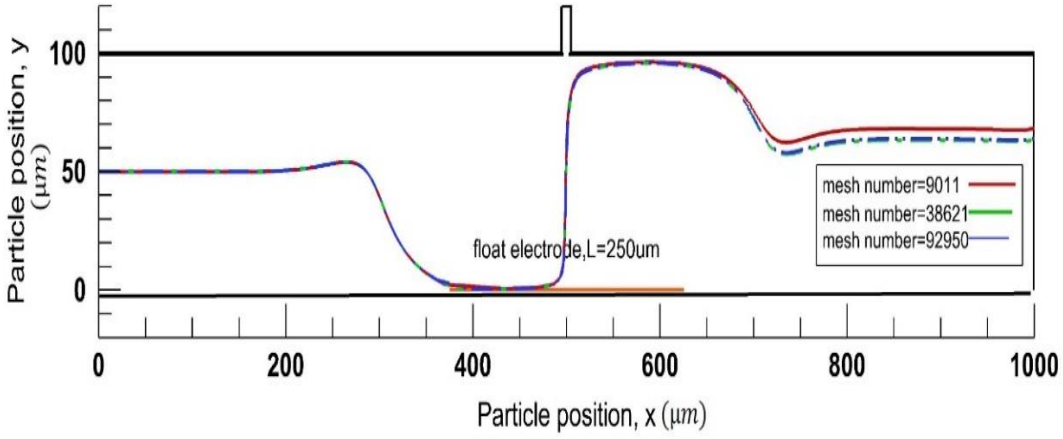

Figure 10. Variations of the particle's trajectory based on the number of different computational grids for the voltage of 80 V and the inlet velocity of 25 $\frac{\mu m}{s}$

The electrical boundary conditions are applied at the input voltage V and zero voltage at the output; the condition of equation (16) is also considered on the floating electrode, which causes eddies of the ICEK phenomenon. The velocity condition for the floating electrode is used from equation (17), and a constant velocity condition is assumed at the input. The point of application of the two outlet conditions is also according to Figure 9.

5. Concluding remarks

As observed in the simulation results, the microparticles are placed inside the vortices of the ICEK phenomenon. Considering that the rotation of both vortices is opposite to each other and the location of the secondary outlet is in the area where the two vortices collide, the microparticles are directed to that area. By adjusting the inlet velocity and the applied voltage, a percentage of the particles can be directed and separated in the direction of the secondary outlet. This adjustable separation using a simple microchip design is one of the innovations of this study.

In the simulation results, it was observed that for input velocities (20-120) $\frac{\mu m}{s}$, with applied voltages (150-330) V (to create an electric field in the floating electrode) and higher voltages, respectively, it was can to direct and separate 100% of the particles towards the secondary outlet.

To validated the simulation results, the results obtained from the simulation method of the present study have been compared with the results of previous works.

Nomenclature

symbol	name	unit
$\vec{\tilde{E}}$	Electric field	V/m
$\vec{x}$	Location	m
t	Time	s
$\vec{u}$	Velocity	m/s
V	Voltage	V
P	Pressure	Pa
f_B	Body force	N/m^3
Re	Reynolds number	——
I	Unique tensor	——
$\vec{F}_{DEP}$	Dielectrophoresis force	N
$Re(\dots)$	Reality part	——
$\vec{n}$	Normal vector	——
R	radius	m
f_{CM}	Clausius-Mossoti factor	——
D	bulk diffusivity	m^2/s
C_d	capacitance of diffuse layer	F/m^2
C_S	capacitance of stern layer	F/m^2
C_0	interfacial total capacitance	F/m^2
m	mass	kg
$\bar{\bar{I}}$	second-order unit tensor	——
I	moment of inertial	m^4
$\vec{T}_{netp}$	total torque acting on the particle	N.m
$\vec{F}_{netp}$	total force acting on the particle	N

Greek symbol

symbol	name	unit
$\tilde{\zeta}$	zeta potential	V
λ_D	Debye screening length	m
ε	Relative permittivity	F/m
ε_0	Vacuum permittivity	F/m
σ	Electrical conductivity	S/m
δ	surface physical capacitance	——
$\tilde{\varphi}$	Electrical potential	V
ω	Angular frequency	Rad/s
τ	double layer relaxation time	s
∇	Gradient	
ρ	Density	kg/m^3
Γ	Surface particle	——

$\bar{\bar{\sigma}}$	Stress Tensor	N/m^2
$\vec{\omega}$	Rotational velocity	1/s
$\vec{\theta}$	orientation	rad
$\bar{\bar{r}}$	size characteristic of the shape	m
Subtitles		
symbol	name	unit
p	Particle	—
f	Fluid	—
DEP	Dielectrophoresis	—
RC	Characteristic RC time	—
slip	slip	—
net	net	—
superscripts		
symbol	name	unit
→	Complex	—
~	Vector	—
*	Conjugate	—

Acknowledgements

We thank the Detection and Tracking Laboratory of Shahrood University of Technology under the management of Dr. Mohsen Nazari for providing the equipment.

Conflicts of Interest

The author declares that there is no conflict of interest regarding the publication of this article.

Data Availability Statement

Data available on request from the authors.

References

[1] Chen, X.-M., Ren, Y., Liu, W., Feng, X., Jia, Y., Tao, Y. and Jiang, H., 2017. A Simplified Microfluidic Device for Particle Separation with Two Consecutive Steps: Induced Charge Electro-osmotic Prefocusing and Dielectrophoretic Separation. 89(17), pp.9583–9592.

[2] Zheng, H., 2013. Using molecular tweezers to move and image nanoparticles. Nanoscale, 5(10), p.4070–78.

[3] Sun, H., Ren, Y., Liu, W., Feng, X., Hou, L., Tao, Y. and Jiang, H., 2018. Flexible Continuous Particle Beam Switching via External-Field-Reconfigurable Asymmetric Induced-Charge Electroosmosis. 90(19), pp.11376–11384.

[4] Manz, A., Harrison, D.Jed., Verpoorte, E.M.J., Fettinger, James.C., Paulus, A., Lüdi, H. and Widmer, H.Michael., 1992. Planar chips technology for miniaturization and integration of separation techniques into monitoring systems. Journal of Chromatography A, 593(1-2), pp.253–258.

[5] Chen, D., Du, H. and Chee Kiang Tay, 2009. Rapid Concentration of Nanoparticles with DC Dielectrophoresis in Focused Electric Fields. 5(1), pp.55–60.

[6] Ho, C.-T., Lin, R.-Z., Chang, W.-Y., Chang, H.-Y. and Liu, C.-H., 2006. Rapid heterogeneous liver-cell on-chip patterning via the enhanced field-induced dielectrophoresis trap. Lab on a Chip, 6(6), p.724.

[7] Bazant, M.Z. and Squires, T.M., 2011. Induced-Charge Electrokinetic Phenomena. pp.221–297.

[8] Peng, C., Lazo, I., Shiyanovskii, S.V. and Lavrentovich, O.D., 2014. Induced-charge electro-osmosis around metal and Janus spheres in water: Patterns of flow and breaking symmetries. 90(5).

[9] Ren, Y., Liu, W., Liu, J., Tao, Y., Guo, Y. and Jiang, H., 2016. Particle rotational trapping on a floating electrode by rotating induced-charge electroosmosis. Biomicrofluidics, 10(5), p.054103.

[10] Ashkin, A., Dziedzic, J.M. and Yamane, T., 1987. Optical trapping and manipulation of single cells using infrared laser beams. Nature, 330(6150), pp.769–771.

[11] Pethig, R., 1996. Dielectrophoresis: Using Inhomogeneous AC Electrical Fields to Separate and Manipulate Cells. Critical Reviews in Biotechnology, 16(4), pp.331–348.

[12] Muller, T., Fiedler, S., Schnelle, T., Ludwig, K., Jung, H. and Fuhr, G., 1996. High frequency electric fields for trapping of viruses. Biotechnology Techniques, 10(4).

[13] Muller, T., Fiedler, S., Schnelle, T., Ludwig, K., Jung, H. and Fuhr, G., 1996. High frequency electric fields for trapping of viruses. Biotechnology Techniques, 10(4).

[14] Liddle, J.A. and Gallatin, G.M., 2011. Lithography, metrology and nanomanufacturing. Nanoscale, 3(7), p.2679.

[15] Zhao, C. and Yang, C., 2018. Continuous-flow trapping and localized enrichment of micro- and nano-particles using induced-charge electrokinetics. Soft Matter, 14(6), pp.1056–1066.

[16] Ding, H., Liu, W., Shao, J., Ding, Y., Zhang, L. and Niu, J., 2013. Influence of Induced-Charge Electrokinetic Phenomena on the

Dielectrophoretic Assembly of Gold Nanoparticles in a Conductive-Island-Basedpp.:12093–12103.

[17] Wu Yupan, Ren, Y., Tao, Y., Hou, L. and Jiang, H., 2016. Large-Scale Single Particle and Cell Trapping based on Rotating Electric Field Induced-Charge Electroosmosis. 88(23), pp.11791–11798.

[18] Ren, Y., Liu, W., Jia, Y., Tao, Y., Shao, J., Ding, Y. and Jiang, H., 2015. Induced-charge electroosmotic trapping of particles. 15(10), pp.2181–2191.

[19] Tao, Y., Ren, Y., Liu, W., Wu Yupan, Jia, Y., Lang, Q. and Jiang, H., 2016. Enhanced particle trapping performance of induced charge electroosmosis. 37(10), pp.1326–1336.

[20] Ren, Y., Liu, J., Liu, W., Lang, Q., Tao, Y., Hu, Q., Hou, L. and Jiang, H., 2016. Scaled particle focusing in a microfluidic device with asymmetric electrodes utilizing induced-charge electroosmosis. Lab on a Chip, 16(15), pp.2803–2812.

[21] Song, Y., Wang, C., Li, M., Pan, X. and Li, D., 2016. Focusing particles by induced charge electrokinetic flow in a microchannel. ELECTROPHORESIS, 37(4), pp.666–675.

[22] Zhao, C. and Yang, C., 2018. Continuous-flow trapping and localized enrichment of micro- and nano-particles using induced-charge electrokinetics. Soft Matter, 14(6), pp.1056–1066.

[23] Ding, H., Liu, W., Shao, J., Ding, Y., Zhang, L. and Niu, J., 2013. Influence of Induced-Charge Electrokinetic Phenomena on the Dielectrophoretic Assembly of Gold Nanoparticles in a Conductive-Island-Based Microelectrode System, pp.12093–103.

[24] Chen, X.-M., Ren, Y., Hou, L., Feng, X., Jiang, T. and Jiang, H., 2019. Microparticle separation using asymmetrical induced-charge electro-osmotic vortices on an arc-edge-based floating electrode. 144(17), pp.5150–5163.

[25] Tavari T, Nazari M, Akbarzadeh P, Sepehry N, Nazari M., 2022. Investigation of electro-osmotic micro-pumps using electrical field gradient and asymmetric micro-electrodes: numerical modeling and experimental validation. Amirkabir journal of mechanical engineering, 54, pp.101–122.

[26] Mottaghi S, Nazari M, Nazari M, Sepehry N, Mahdavi A., 2021. Control of droplet size in a two-phase microchannel using PID controller: A novel experimental study. Amirkabir journal of mechanical engineering, 53, pp.4279–4292.

[27] Baylon-Cardiel, J.L., Jesús-Pérez, N.M., Chávez-Santoscoy, A.V. and Lapizco-Encinas, B.H., 2010. Controlled microparticle manipulation employing low frequency alternating electric fields in an array of insulators. 10(23), pp.3235–3242.

[28] Wu, Z. and Li, D., 2007. Mixing and flow regulating by induced-charge electrokinetic flow in a microchannel with a pair of conducting triangle hurdles. Microfluidics and Nanofluidics, 5(1), pp.65–76.

[29] Wu, Z. and Li, D., 2008. Micromixing using induced-charge electrokinetic flow. Electrochimica Acta, 53(19), pp.5827–5835.

[30] Tavari, T., Nazari, M., Meamardoost, S., Tamayol, A. and Samandari, M., 2022. A systematic overview of electrode configuration in electric-driven micropumps. *Electrophoresis*, *43*(13-14), pp.1476-1520.

[31] Tavari, T., Meamardoost, S., Sepehry, N., Akbarzadeh, P., Nazari, M., Hashemi, N.N. and Nazari, M., 2023. Effects of 3D electrodes arrangement in a novel AC electroosmotic micropump: Numerical modeling and experimental validation. *Electrophoresis*, *44*(3-4), pp.450-461.

[32] Nazari, M., Rashidi, S., Abolfazli Esfahani, J. and Harmand, S., 2022. A novel electrokinetic micromixing system with conductive mixing-enclosure-A geometrical study. *Journal of Heat and Mass Transfer Research*, *9*(1), pp.65-76.

[33] Nazari, M., Rashidi, S. and Esfahani, J.A., 2020. Effects of flexibility of conductive plate on efficiency of an induced-charge electrokinetic micro-mixer under constant and time-varying electric fields-A comprehensive parametric study. Chemical Engineering Science, 212, p.115335.

[34] Daghighi, Y., Gao, Y. and Li, D., 2011. 3D numerical study of induced-charge electrokinetic motion of heterogeneous particle in a microchannel. *Electrochimica acta*, *56*(11), pp.4254-4262.

[35] Nazari, M., Chuang, P.-Y.A., Abolfazli Esfahani, J. and Rashidi, S., 2020. A comprehensive geometrical study on an induced-charge electrokinetic micromixer equipped with electrically conductive plates. International *Journal of Heat and Mass Transfer*, 146, p.118892.

[36] Azimi, S., Nazari, M. and Daghighi, Y., 2017. Developing a fast and tunable micro-mixer using induced vortices around a conductive flexible link. Physics of Fluids, 29(3), p.032004.

[37] Nazari, M., Rashidi, S. and Esfahani, J.A., 2019. Mixing process and mass transfer in a novel design of induced-charge electrokinetic micromixer with a conductive mixing-chamber. International Communications in Heat and Mass Transfer, 108, p.104293.